Numerical Detection and Continuation of Saddle-node Homoclinic Bifurcations of Codimension One and Two

Fengshan Bai[*] & A.R. Champneys[†]

School of Mathematical Sciences,

University of Bath,

Bath BA2 7AY, U.K.

email: a.r.champneys@bristol.ac.uk

Abstract

An extension of an existing truncated boundary-value method for the numerical continuation of connecting orbits is proposed to deal with homoclinic orbits to a saddle-node equilibrium. In contrast to previous numerical work by Schecter and Friedman & Doedel, the method is based on (linear) projection boundary conditions. These boundary conditions, with extra defining conditions for a saddle-node, naturally allow the continuation of codimension-one curves of saddle-node homoclinic orbits. A new test function is motivated for detecting codimension-two points at which loci of saddle-nodes and homoclinic orbits become detached. Two methods for continuing such codim 2 points in three parameters are discussed. The numerical methods are applied to two example systems, modelling a DC Josephson Junction and CO-oxidation. For the former model existing numerical results are recovered and extended; for the latter, new dynamical features are uncovered. All computations are performed using AUTO.

1 Introduction

The aim of this paper is to continue the development, begun in (Champneys & Kuznetsov 1993), of a robust numerical continuation framework for the analysis of homoclinic bifurcations

[*]Address from Feb 1994: Applied Mathematics Department, Tsinghua University, Beijing, 100084, P.R.China

[†]Permanent address: Department of Engineering Mathematics, University of Bristol, Bristol, BS8 1TR, UK

in parametrized systems of autonomous ordinary differential equations (ODEs). The specific case under investigation here is solutions that are bi-asymptotic to an equilibrium with a zero eigenvalue; *saddle-node homoclinic orbits*. Given a hyperbolic equilibrium (i.e. a steady state whose linearisation does not contain eigenvalues on the imaginary axis) then a homoclinic orbit to that equilibrium is generically of *codimension one* (i.e. a single problem parameter needs to be varied in order to see it). Thus the existence of a homoclinic orbit gives rise to a global bifurcation, which property causes them to be fundamental to understanding complex dynamical behaviour of model systems. Homoclinic orbits (and their counterparts, heteroclinic orbits) are also of importance as they describe the profiles of travelling solitary waves solutions of evolution partial differential equations. See Gaspard, Arnéodo, Kapral & Sparrow (1993) for a flavour of the diversity of applications of homoclinic phenomena.

In problems with two (or more) control parameters, a key to understanding the global dynamics associated with homoclinic orbits is to identify and analyze degenerate, or *codimension-two*, homoclinic orbits that occur at isolated points along a codimension-one homoclinic locus in parameter space. In Champneys & Kuznetsov (1993) all known codim 2 homoclinic orbits that involve a unique homoclinic orbit to a hyperbolic equilibrium were surveyed and a numerical test function for each kind of degeneracy was derived. It was shown how these test functions could be used to detect the codim 2 points in question while continuing, in two parameters, a codim 1 locus of homoclinic orbits using a known numerical method (Beyn 1990*b*). This method involves solving a boundary-value problem over an approximation $[T_-, T_+]$, $T_+ - |T_-| = T$, to the infinite time-interval, with (linear) projection boundary conditions onto the stable and unstable eigenspaces of the equilibrium (Beyn 1990*b*). It was also shown how to continue codim 2 homoclinic orbits in three or more parameters using similar methods, and how to implement the whole procedure using AUTO (Doedel (1981),Doedel, Keller & Kernévez,(1991*a*, 1991*b*)).

Also reviewed in Champneys & Kuznetsov (1993) were two separate cases of codimension-two homoclinic orbits involving non-hyperbolic equilibria. These cases are identified by a locus of homoclinic orbits colliding with a locus of local bifurcations of the equilibrium; either a Hopf bifurcation (corresponding to eigenvalues $\pm i\omega$), or a saddle-node (corresponding to a simple zero eigenvalue). It was argued that the existing numerical method could be used to continue approximations to homoclinic solutions through the former degeneracy, and thus allow for the detection of the codim 2 point, but not in the latter case. There are sound theoretical reasons why saddle-node homoclinic orbits should present this difficulty (see below) and the specific aim of the present paper is to enable saddle-node homoclinic orbits to be treated numerically on the same footing as other codim 2 homoclinic bifurcations.

Figure 1: Saddle-node homoclinic bifurcation portrait.

Naively, one might assume that a homoclinic orbit to a saddle-node should always be of codimension two, because two codim 1 phenomena (namely a homoclinic orbit and a saddle-node) occur simultaneously. It is perhaps not as widely known as it should be that this is *not* the case; that saddle-node homoclinic orbits are typically of codimension-one. There is, however, a codimension-two bifurcation caused by the transition between a homoclinic orbit to a hyperbolic equilibrium and to a saddle node (see Figure 1). At such a point, (O in Figure 1), a locus of hyperbolic homoclinic orbits can be thought to collide with and *glue onto* a locus of saddle-node bifurcations.

The difference between codim 1 and codim 2 saddle-node homoclinic orbits is in their asymptotic behaviour as they approach the equilibrium (compare the phase portraits 5 and 3 in Figure 1). A codim 1 orbit is tangent to the center eigenspace (i.e. the eigenvector associated with the zero eigenvalue) as t tends to both $+\infty$ and $-\infty$, whereas the codim 2 orbit is tangent to the center manifold only in one of these limits. Consequently, we call the former a center-to-center connection and the latter a center-to-stable or unstable-to-center connection.

The analysis of saddle-node homoclinic orbits, leading to the conclusion that Figure 1 is generic, dates back to Lukyanov (1982) and Schecter (1987) for planar systems, and has been extended to the general case by Chow & Lin (1990) and Deng (1990).

Recently Friedman & Doedel (1993) and Friedman (1993) have proposed, analysed and applied an extension to their algorithm for heteroclinic connections between hyperbolic equilibria to deal with cases where at least one equilibrium is non-hyperbolic (see also Schecter (1993)). The key idea is to define approximate boundary conditions which use linear approximations to the stable and unstable manifolds, but which incorporate a higher-order approximation to the center manifold. This approach was motivated by the fact that the error estimate for homoclinic solutions and parameter values using the existing methods, which are $O(e^{-kT})$ for constants k relating to the eigenvalues of the equilibrium, become $O(1)$ for a non-hyperbolic equilibrium (Beyn 1990*b*, Friedman & Doedel 1991, Schecter 1993, Schecter 1994). We note two drawbacks of Friedman and Doedel's method applied to saddle-node homoclinic orbits. First it is not clear how to incorporate the higher-order approximations to invariant manifolds as projection boundary conditions (see the discussion in Champneys & Kuznetsov (1993) concerning the advantages for homoclinic continuation purposes of projection boundary conditions against "explicit" boundary conditions). Second, and more seriously, Friedman and Doedel's method is not designed for the continuation of codim 1 curves of saddle-node homoclinic orbits. In the example on which they illustrate their method (a DC Josephson Junction, see also Section 4.1, below) they were only able to approach a codim 2 center-to-stable connection, *by following a locus of homoclinic orbits to hyperbolic equilibria*. It is these two drawbacks that the method of the present paper seeks to overcome.

In Section 2 we state the mathematical problem of homoclinic orbits to hyperbolic and non-hyperbolic equilibria. Then, in Section 3.1 we present our numerical method, which is based on using (linear) projection boundary conditions. The algorithm differs from that for hyperbolic equilibria, because the boundary conditions allow the numerical solution to have components in the center eigenspace at both endpoints. The above discussion on error estimates suggests that using merely a linear approximations to the center manifold may be naive. However a conjecture of Schecter (1994) and some numerical results of Friedman & Doedel (1993) (for the center-unstable case) suggests that, in practice, the true error in the numerically obtained parameter values using a linear approximation to the center manifold, decays exponentially with

T, and that the error for the homoclinic solution behaves like $(1/T^2)$. We present no analysis here to support this claim, but our numerical results strongly suggest that linear boundary conditions, in practice, suffice.

Section 3.2 concerns algorithms for detection of codim 2 saddle-node homoclinic orbits. The ideal aim would be for a continuation code to treat codim 2 saddle-node homoclinic orbits on the same footing as the other cases considered in Champneys & Kuznetsov (1993); namely to have the ability to continue a codim 1 locus of homoclinic orbits through the degeneracy, with accurate detection of the codim 2 point. The drawback for saddle-node homoclinic orbits is that one has to use different boundary conditions for the hyperbolic and non-hyperbolic orbits. The next best thing, as proposed in Section 3.2, is to be able to detect the codimension-two point by following *either* kind of orbit, i.e. to find points where a locus of hyperbolic homoclinic orbits sticks onto a saddle-node locus, or where glued saddle-node and homoclinic loci become unstuck. We also allow for branch-switching at the codim 2 point, and to follow the codim 2 point in three or more parameters.

In Section 4 we illustrate our numerical methods by presenting numerical results on two example systems. The first example is the two-dimensional model of a DC Josephson Junction that is studied in Friedman & Doedel (1993). The second example is a three-dimensional model of CO-oxidation ((Bykov, Yablonski & Kim 1978, Khibnik 1990)). Finally, in Section 5 we draw conclusions and discuss a few unresolved issues.

2 Saddle-node Homoclinic Orbits

In this paper we consider sufficiently smooth, generic dynamical systems of the form

$$\dot{x} = f(x, \alpha), \quad x \in \mathbb{R}^n, \ \alpha \in \mathbb{R}^p. \tag{2.1}$$

Suppose that at some parameter value $\alpha = \alpha^*$, say, there is an orbit Γ of (2.1) that is homoclinic to an equilibrium x^*. That is,

$$\Gamma = \{\gamma(t) \mid t \in \mathbb{R}\}, \quad \text{where} \quad \lim_{t \to \pm\infty} \gamma(t) = x^*. \tag{2.2}$$

We further assume that

$(H.0)$ Γ *is the only orbit homoclinic to* x^* *at* $\alpha = \alpha^*$.

Suppose that $A = (D_x f)(x^*, \alpha^*)$ has n_s eigenvalues μ_i, $i = 1, \ldots, n_s$, with non-positive real part and n_u eigenvalues λ_i, $i = 1, \ldots, n_u$, with positive real part (counting multiplicities), such that

$$n_u + n_s = n,$$

$$\mathrm{Re}\{\mu_{n_s}\} \leq \ldots \leq \mathrm{Re}\{\mu_2\} \leq \mathrm{Re}\{\mu_1\} \leq 0 < \mathrm{Re}\{\lambda_1\} \leq \mathrm{Re}\{\lambda_2\} \ldots \leq \mathrm{Re}\{\lambda_{n_u}\}.$$

In Champneys & Kuznetsov (1993) it was further assumed that

$(H.1)$ *the equilibrium is hyperbolic*: $\mathrm{Re}\{\mu_1\} \neq 0$.

Here we shall be interested also in the case where

$(H.1)'$ *the equilibrium is a saddle-node*: $\mu_1 = 0$, $\mathrm{Re}\{\mu_2\} \neq 0$.

Remark The condition for the equilibrium to be a saddle-node, rather than a pitchfork or transcritical bifurcation, requires extra non-degeneracy conditions on $f(x^*, \alpha^*)$ (see Deng (1990)). We shall not consider the cases of pitchfork or transcritical non-center-to-center homoclinic bifurcation, because these are actually of codim 3 for generic dynamical systems.

If x^* is hyperbolic, the stable and unstable manifolds $W^s(x^*)$, $W^u(x^*)$ of x^* are defined by

$$W^s(x^*) \quad = \quad \{x \in \mathbb{R}^n \mid \phi^t(x) \to x^* \text{ as } t \to +\infty\}, \tag{2.3}$$

$$W^u(x^*) \quad = \quad \{x \in \mathbb{R}^n \mid \phi^t(x) \to x^* \text{ as } t \to -\infty\}, \tag{2.4}$$

where ϕ^t is the flow of (2.1).

Definition 2.1 *A homoclinic orbit to a hyperbolic equilibrium is called* regular *if* $(H.0)$ *and* $(H.1)$ *hold and additionally*

$$(H.2) \qquad codim\left(T_{\gamma(t)}W^s(x^*) + T_{\gamma(t)}W^u(x^*)\right) = 1,$$

Remark The condition $(H.2)$ can be expressed analytically in terms of (2.1) (see Beyn (1990*a*)).

For the case of x^* being non-hyperbolic, specifically a saddle-node, we need to consider the center-stable and center-unstable manifolds $W^{cs}(x^*)$, $W^{cu}(x^*)$ which are smooth invariant manifolds that are tangent, at $x = x^*$, to the center + stable and center + unstable eigenspaces respectively (see Deng (1990) and references therein for definitions and properties of these manifolds in the present context).

Definition 2.2 *A homoclinic orbit to a saddle-node is called* regular *if* $(H.0)$ *and* $(H.1)'$ *hold and*

$$(H.2)' \qquad W^{cu}(x^*) \quad \textit{and} \quad W^{cs}(x^*) \quad \textit{intersect transversally along} \quad \gamma(t).$$

For a smooth dynamical system (2.1), depending smoothly on its parameters, the parameter values at which regular homoclinic orbits (according to either Definition 2.1 or 2.2) exist, form smooth sub-manifolds of codim 1 in parameter space. A sub-manifold $\mathcal{H}^{(1)}$ of hyperbolic homoclinic orbits can be partitioned into regions $\mathcal{H}_i^{(1)}$ within which qualitatively similar bifurcation scenarios occur upon a transversal crossing of $\mathcal{H}_i^{(1)}$. The boundaries of each $\mathcal{H}_i^{(1)}$ are determined by certain non-degeneracies conditions failing and give rise to codim 2 homoclinic bifurcations. Some such codim 2 bifurcations were considered in Champneys & Kuznetsov (1993). In this paper we are concerned with the violation of $(H.1)$, specifically due to $(H.1)'$. Such a degeneracy corresponds to a boundary of the sub-manifold $H^{(1)}$, which boundary is shared with a smooth codim 1 sub-manifold $\mathcal{H}^{(0)}$ of homoclinic orbits to saddle-nodes. As in the hyperbolic case, one could presumably define non-degeneracy conditions for saddle-node homoclinic orbits that divide a sub-manifold $\mathcal{H}^{(0)}$ into regions of qualitative similar dynamics. We do not pursue such codimension-two bifurcations of saddle-node homoclinic orbits here. Instead we shall be interested in computing a boundary of $\mathcal{H}^{(0)}$ caused by the failure of the condition $(H.2)'$. Specifically where

$$\Gamma \subset W^{cu} \cap W^{s} \quad \text{or} \quad \Gamma \subset W^{u} \cap W^{cs}. \tag{2.5}$$

Note that condition $(H.1)'$ applied to a sub-manifold $\mathcal{H}^{(1)}$ and condition (2.5) applied to a sub-manifold $\mathcal{H}^{(0)}$ generically define the same codim 2 sub-manifold; namely that corresponding to a transition between hyperbolic and saddle-node homoclinic orbits as depicted in Figure 1.

3 Numerical Methods

3.1 Continuation of saddle-node homoclinic orbits

In this section we review a numerical method for the computation of homoclinic orbits that are regular according to Definition 2.1 and extend this method to deal with homoclinic orbits to saddle-nodes (i.e. regular according to Definition 2.2). We do not give any theoretical basis for these methods, but refer the reader to Beyn (1990*a*, 1990*b*), Friedman & Doedel (1991, 1993) and Schecter (1993, 1994) for convergence proofs and error estimates. Recall from the Introduction, however, that we know of no error analysis to support our method for saddle-node homoclinic orbits.

Our aim is to compute loci of orbits in sub-manifolds $\mathcal{H}^{(0),(1)}$ as two parameters are varied, using numerical continuation. We do not give details of the continuation here, but remark that the base step in a two-parameter continuation algorithm is the solution of a one-parameter problem (see e.g. Doedel, Keller & Kernévez (1991*a*, 1991*b*) for more details). For simplicity then, we suppose that there is a single active parameter $\alpha \in \mathbb{R}$ and seek a solution $(x, \alpha) \in C^1(\mathbb{R}, \mathbb{R}^n) \times \mathbb{R}$, satisfying

$$\dot{x} = f(x(t), \alpha), \tag{3.1}$$

$$x(t) \to x^*, \quad \text{as } t \to \pm\infty. \tag{3.2}$$

Note that, (3.1), (3.2) is an ill-posed problem because any time shift of a solution is still a solution. There are variety of phase conditions one can use, but we shall use the following global one

$$\int_{-\infty}^{+\infty} \dot{\bar{x}}^T(t)[x(t) - \bar{x}(t)]dt = 0, \tag{3.3}$$

(Doedel 1981), in which $\bar{x}$ is some initial guess for the homoclinic solution. The condition (3.3) is a necessary condition for a minimum of the L_2-distance between x and $\bar{x}$ over time shifts.

The boundary-value problem (3.1)-(3.3), defined on an infinite time domain, can be solved by truncating to a finite interval $[T_-, T_+]$ and imposing suitable boundary conditions at T_- and T_+. For the case of x^* being hyperbolic, the following projection boundary conditions were shown by Beyn (1990*b*, 1990*a*) to be optimal among linear boundary conditions. Let $L_s(\alpha)$ and $L_u(\alpha)$ be matrices such that their rows form a basis for the stable and unstable eigenspaces respectively of $A^T(\alpha) = (D_x f)^T(x^*, \alpha)$. Hence the projection boundary conditions are

$$L_s(\alpha)(x(T_-) - x^*) = 0, \tag{3.4}$$

$$L_u(\alpha)(x(T_+) - x^*) = 0, \tag{3.5}$$

and the phase condition for the truncated problem is taken to be

$$\int_{T_-}^{T_+} \dot{\bar{x}}^T(t)[x(t) - \bar{x}(t)]dt = 0. \tag{3.6}$$

It is well known that x^* being hyperbolic (i.e. on a homoclinic sub-manifold $\mathcal{H}^{(1)}$) implies

$$L_s(\alpha) \in \mathbb{R}^{n \times n_s}, \qquad L_u(\alpha) \in \mathbb{R}^{n \times n_u}, \tag{3.7}$$

with $n_s + n_u = n$. Hence (3.4), (3.5) together with (3.6) give n boundary conditions and one integral constraint for the equation (3.1), which gives a well defined codimension-one problem.

Consider now the case where x^* is a saddle-node, i.e. on homoclinic sub-manifold $\mathcal{H}^{(0)}$. Then, instead of (3.7), we have

$$L_s(\alpha) \in \mathbb{R}^{n \times (n_s - 1)}, \qquad L_u(\alpha) \in \mathbb{R}^{n \times n_u}.$$

Hence (3.4) and (3.5) now give only $(n-1)$ boundary conditions for the equation (3.1) (which is because the solution $x(t)$ is allowed to have components in the center eigenspace at *both* the endpoints). However, in the present case, we know additionally that x^* is a saddle-node, which can be expressed by the following defining conditions:

$$f(x^*, \alpha^*) = 0, \tag{3.8}$$

$$(D_x f)(x^*, \alpha^*) v_1 = 0, \tag{3.9}$$

$$v_1^T v_1 - 1 = 0. \tag{3.10}$$

Here v_1 is the eigenvector of $(D_x f)$ corresponding to the eigenvalue 0. Using (3.8)–(3.10) we can now solve for x^* and α^* at the same time as solving (3.1), (3.4)–(3.6) for the homoclinic orbit.

A quick count shows that to compute an orbit in $\mathcal{H}^{(0)}$, (and also at the codim 2 boundary between $\mathcal{H}^{(1)}$ and $\mathcal{H}^{(0)}$), one gets n differential equations (3.1), with $(n-1)$ { projection boundary conditions (3.4) and (3.5) } +1 { phase condition (3.6) } $+(2n+1)$ { extra algebraic boundary conditions (3.8)–(3.10) } =(3n+1) boundary conditions and $2n$ extra parameters (x^* and v_1). Hence the number of unknowns is one less than the number of fixed conditions, which gives a well defined problem of codimension 1.

3.2 Detection and continuation of codim 2 points

We wish to define test functions for the detection of saddle-node homoclinic orbits. A test function is a smooth scalar function defined in a neighbourhood of a solution branch $(x^*(s), \alpha^*(s))$ of either (3.1), (3.4)–(3.6) or (3.1), (3.4)–(3.6), (3.8)–(3.10), which has a regular zero at the degeneracy. Once a test function has been defined it can be monitored during the continuation process and a zero detected accurately.

First we consider the case of the detection of a saddle-node upon following a locus $\mathcal{H}^{(1)}$ of hyperbolic homoclinic orbits. Here we can use condition $(H.1)'$. To be completely general, we want to allow for either a positive or negative eigenvalues to become zero, therefore we take the two separate test functions proposed in Champneys & Kuznetsov (1993), namely

$$\psi_9 = \mathrm{Re}\{\mu_1\},$$

$$\psi_{10} = \mathrm{Re}\{\lambda_1\}.$$

Recall, however, with reference to Figure 1 and Champneys & Kuznetsov (1993) that the boundary-value problem (3.1), (3.4)–(3.6) cannot be used to follow orbits through a codim 2 saddle-node homoclinic point, hence $\psi_{9,10}$ *cannot* be used as reliable test functions. Nonetheless, by monitoring $\psi_{9,10}$ one can gain estimates (perhaps by extrapolation) of the location of the codim 2 point.

We now turn our attention to loci $\mathcal{H}^{(0)}$ of homoclinic orbits to saddle-nodes. The aim here is to detect a degeneracy given by (2.5). With reference to Figure 1 note that we are in a slightly better situation here, because although the locus $\mathcal{H}^{(2)}$ ceases to exist on the far side of O, there is an approximate solution to (3.1), (3.4)–(3.6), (3.8)–(3.10) on the far side of O. Specifically, sufficiently close to O along the continuation of $\mathcal{H}^{(0)}$ (phase portrait 7 in Figure 1), there is a solution that lies in the stable manifold at $t = T_-$ and which is close to the center manifold at $t = T_+$. Note, however, that this solution lies in the opposite component of the center manifold to the homoclinic solution on $\mathcal{H}^{(0)}$ (cf. phase portraits 3 and 7 in Figure 1). Hence we can define two test functions for detecting codim 2 saddle-node homoclinic points

$$\psi_{sn1} = (x(T_+) - x^*)^{\mathrm{T}} v_1, \tag{3.11}$$

$$\psi_{sn2} = (x(T_-) - x^*)^{\mathrm{T}} v_1. \tag{3.12}$$

Recall that v_1 is the eigenvector of $D_x f$ corresponding to the eigenvalue 0. Hence (3.11) and (3.12) measure the component of the one-dimensional center manifold in which the two endpoints of the approximate homoclinic orbit lie. On crossing a codim 2 point (such as at O in Figure 1) the above arguments explain why we expect one of these test functions to change sign (the choice of which one changes being determined by whether the critical homoclinic orbit is a center-to-stable or unstable-to-center connection). Also, due to the continuous dependence of solutions over *finite* time intervals, we expect (3.11) and (3.12) to be smooth functions of x and α in a neighbourhood of the codim 2 point.

Once a zero of a test function has been located (either accurately or by extrapolation) in a continuation process, one possibility is to switch to following the other locus of homoclinic orbits. Given that the data for the homoclinic orbit at the codim 2 point would be already known, one would only be required to switch the set of boundary conditions; e.g. from (3.4)–(3.6) for computing homoclinic orbits to a hyperbolic equilibrium to (3.4)–(3.6), (3.8)–(3.10) for computing homoclinic orbits to a saddle-node. Notice that (3.4) gives one less boundary condition for the later case. Another possibility upon detecting a codim 2 point would be to compute a locus of such codim 2 points in three parameters. Here one adds an appropriate condition $\psi = 0$ to the problem being solved, while allowing another problem parameter to vary. Notice that this gives two possible algorithms for continuing a codim 2 saddle-node homoclinic orbit; either (3.1), (3.4)–(3.6), (3.8)–(3.10) with the extra condition $\psi_{sn1} = 0$ (or $\psi_{sn2} = 0$), or (3.1), (3.4)–(3.6) with extra condition $\psi_9 = 0$ (or $\psi_{10} = 0$). In the latter case, we assume (3.7), i.e. include the zero eigenvalue in either the stable or the unstable eigenspace depending on whether we seek an unstable-to-center or a center-to-unstable connection.

4 Examples and Numerical Results

All the computations in this paper are performed using the software package AUTO written by E. Doedel (see Doedel (1981), Doedel, Keller & Kernévez (1991*a*, 1991*b*) for details). We implement our approach, in particular evaluate our boundary conditions and test functions, in the similar manner to that discussed in Section 5.1 of Champneys & Kuznetsov (1993). To solve for homoclinic orbits, we use AUTO to compute paths of solutions to boundary value problem with integral constraints and non-separated boundary conditions, at each continuation step computing the eigenvalues and eigenvectors of $Df(x^*)$ using a NAG routine.

To start the continuation of loci of homoclinic orbits, initial approximations are needed. Various strategies for doing this are possible (e.g. Doedel, Friedman & Monteiro (1993); see Champneys & Kuznetsov (1993) and references therein), and we remark that the use of shooting to locate homoclinic orbits can be extended to saddle-node homoclinic orbits (Kaas-Peterson & Scott 1988). In the computations which follow, the initial approximations for homoclinic orbits are obtained by following periodic solutions, which typically bifurcate from certain Hopf bifurcation points, to large period (sometime we need to perform a time shift on the data from a periodic orbit).

4.1 DC Josephson Junction

A model for a DC Josephson junction can be expressed in the form (Schecter 1987, Friedman & Doedel 1993):

$$\dot{x_1} = x_2, \tag{4.1}$$

$$\dot{x_2} = \frac{1}{\beta}(-x_2 - \sin x_1 + \rho). \tag{4.2}$$

Notice that if we identify x_1 and $x_1 + 2\pi$, then (4.1) and (4.2) define a vector field on a cylinder, and a heteroclinic orbit between equilibria $(x_1, x_2) = (\pi, -\text{arcsin}\rho)$ and $(3\pi, -\text{arcsin}\rho)$ can be regarded as a homoclinic orbit in this phase space. The bifurcation diagram is exactly as shown schematically in Figure 1, with the horizontal parameter being $\rho - 1$ and the vertical parameter $\beta - \beta^*$, for some value of β^*.

The computations performed by Friedman & Doedel (1993) were as follows. For the homoclinic orbit at a point on $\mathcal{H}_1^{(1)}$, an approximation was obtained by following a nearby periodic solution to large period. Continuation of the homoclinic orbits along $\mathcal{H}_1^{(1)}$ in the direction approaching the codimension 2 point O was then carried out using a method analogous to (3.1), (3.5)–(3.7), namely explicit (rather than projection) linear boundary conditions. Using this method with $T = 121.3$ they estimate the codim 2 point as being at $(\sqrt{1-\rho}, \beta) = (10^{-6}, 0.7025648)$. The continuation of $\mathcal{H}_1^{(1)}$ towards O was also repeated using second- third- and fourth-order approximations to the unstable manifold. It was however found that the higher-order approximations made little difference to the numerically observed error dependence on T.

Here, we have repeated the calculations in Friedman & Doedel (1993), using the method for homoclinic orbits to hyperbolic equilibria outlined in Section 3.1. Using a value of $T = 10^3$ and linear projection boundary conditions, a sufficiently accurate estimate of the codim 2 point was computed (before AUTO failed to converge) to be used as a start point for the computation of the locus of codim 1 homoclinic orbits to a saddle-node along $\mathcal{H}_1^{(0)}$. The latter computation was performed by switching to the extended system (3.1) (3.4)–(3.6), (3.8)–(3.10). Figure 2 shows the bifurcation diagram so computed; homoclinic orbits at points labelled by $1, 2, 3$ are plotted in Figure 3. Figure 3(a) shows a homoclinic orbit at the codimension two saddle-node point O with $\rho = 1.0, \beta = 0.7025639$, labelled by 2 in Figure 2; Figure 3(b) shows a homoclinic orbit on $\mathcal{H}_1^{(0)}$ with $\rho = 1.0, \beta = 0.3982878$, (label 1); Figure 3(c) shows a homoclinic orbit on $\mathcal{H}_1^{(1)}$ with $\rho = 0.9643271, \beta = 1.0$, (label 3).

We have also been able to perform the computation in reverse. Namely, to detect and switch branches at the codim 2 point by following the locus of saddle-node homoclinic orbits. To obtain an initial point on $\mathcal{H}_1^{(0)}$, an approximation was obtained by following a nearby periodic solution to large period. We then continued the homoclinic orbits along $\mathcal{H}_1^{(0)}$ in the direction approaching the codimension 2 point O. A zero of the test function ψ_{sn1} was detected at $(\rho, \beta) = (1.00000000000, 0.70256568975)$. At this point, we switched boundary conditions to compute the locus of homoclinic orbits along $\mathcal{H}_1^{(1)}$. The results obtained were identical to those displayed in Figures 2, 3

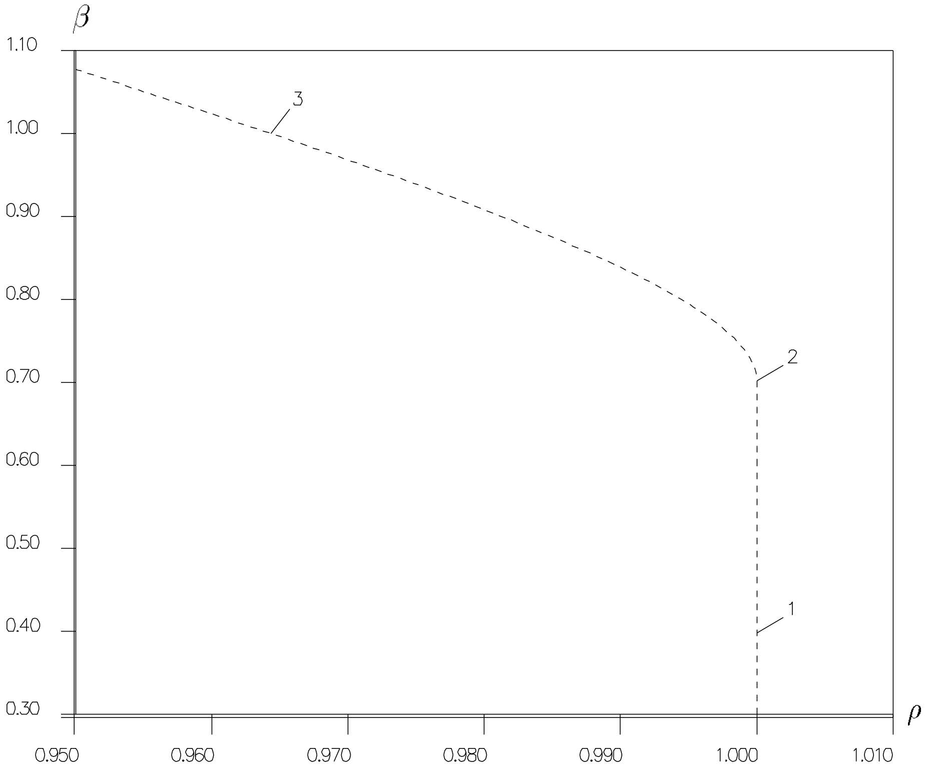

Figure 2: Bifurcation diagram in parameter space for the DC Josephson junction model.

4.2 CO-oxidation

A model for CO-oxidation was derived by Bykov et al. (1978) (see also (Khibnik 1990, Beyn 1992) for more details on its dynamics):

$$\dot{x} = 2k_1 z^2 - 2k_{-1}x^2 - k_3 xy \tag{4.3}$$

$$\dot{y} = k_2 z - k_{-2} y - k_3 xy \tag{4.4}$$

$$\dot{s} = k_4(z - \frac{k_{-4}}{k_4} s) \tag{4.5}$$

where $z = 1 - x - y - s$. The dynamics of this problem are less well understood problem than (4.1), (4.2). First, we consider the case where five reaction constants are fixed at

$$k_1 = 2.5, \quad k_{-1} = 1, \quad k_3 = 10, \quad k_{-2} = 0.1, \quad k_4 = 0.0675,$$

with the bifurcation parameters taken to be

$$\alpha_1 = k_2; \quad \alpha_2 = \frac{k_{-4}}{k_4}.$$

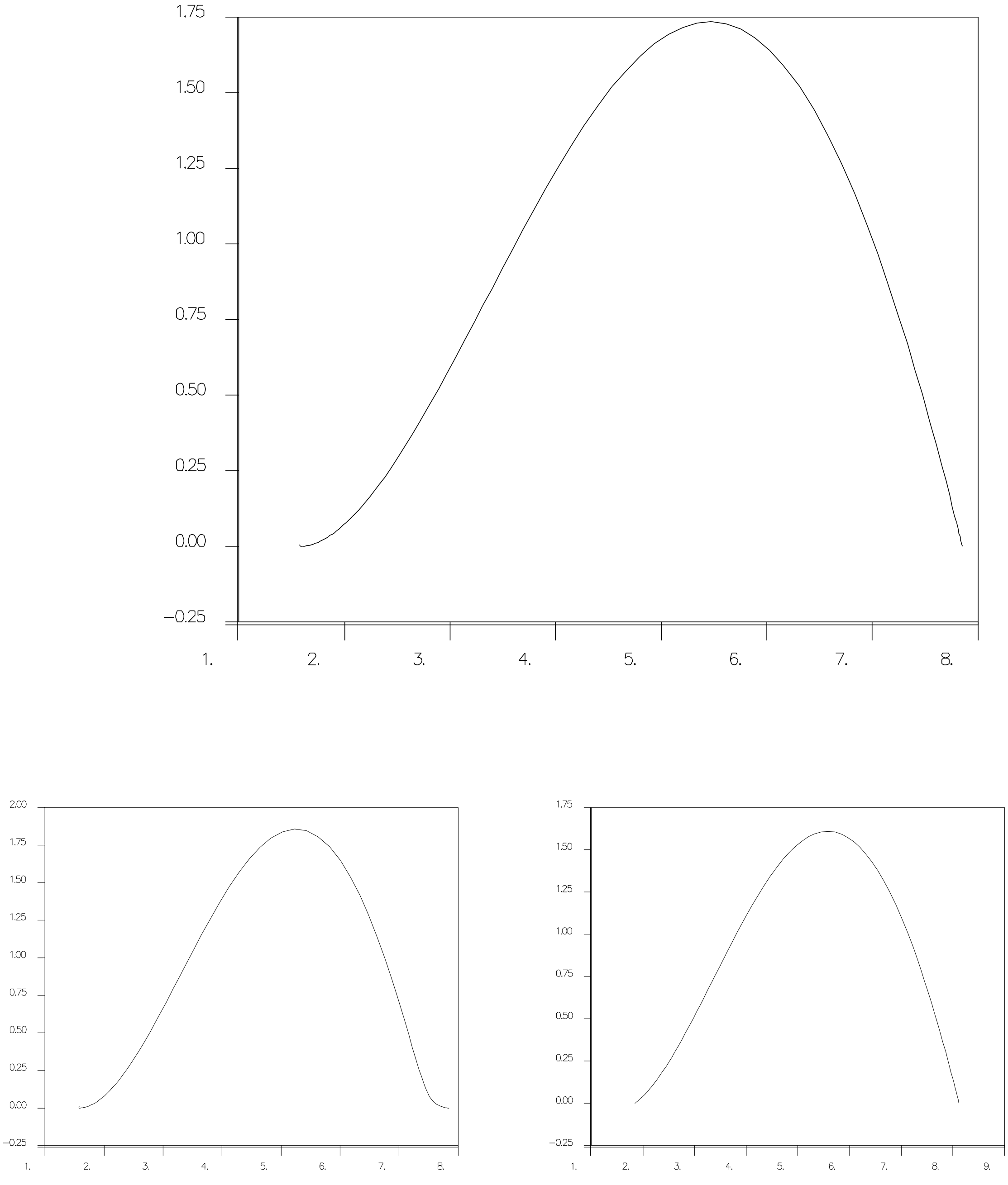

Figure 3: Homoclinic orbits for the DC Josephson junction (x_1 as abscissa, x_2 as ordinate); (a) the codimension-two saddle-node homoclinic orbit, (b) a saddle-node homoclinic orbit on $\mathcal{H}^{(0)}$, (c) an orbit homoclinic to a hyperbolic equilibrium on $\mathcal{H}^{(1)}$.

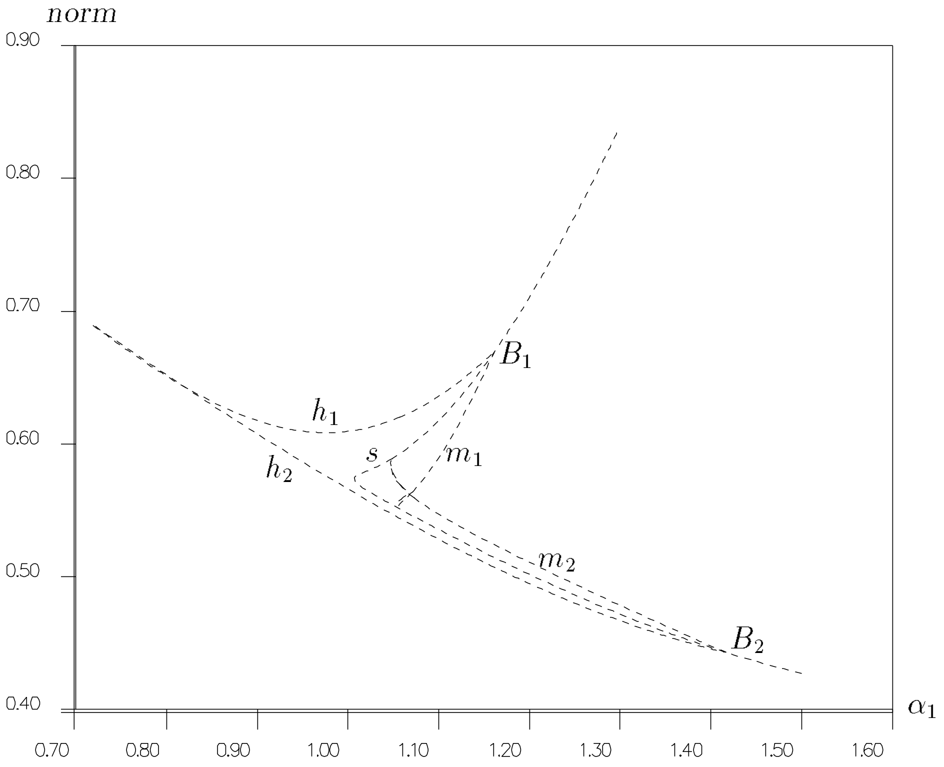

Figure 4: Projection onto the (α_1,norm)-plane of the two-parameter bifurcation diagram for CO-oxidation.

Figures 4–6 depict the global two-parameter bifurcation diagram for these values, which were computed using the standard local bifurcation features of AUTO and the method for hyperbolic homoclinic orbits reviewed in Section 3 (many local bifurcation curves have already been computed by Khibnik (1990)). Figure 4 depicts the norm of solutions against the single parameter α_1, whereas Figures 5 and 6 (Figure 6 is a blow-up of a small portion of Figure 5) depict bifurcation loci in the (α_1, α_2)-plane. The norm used in Figure 4 is the L_2 norm of the solution $(x(t), y(t), s(t)) \in \mathbb{R}^3$. We shall now explain the results.

The points labelled by B_1 and B_2 are two Takens–Bogdanov (T.B.) points, near $(\alpha_1, \alpha_2) = (1.160, 0.716)$ and $(1.415, 0.965)$, the latter point is the one computed by Beyn (1992). We didn't compute these points exactly but can infer their existence from the bifurcation diagrams in their neighbourhood. Curves labelled h_1 and h_2 in Figure 4 are loci of Hopf bifurcation points; and that labelled s is a locus of saddle-nodes. From Figure 5, which is in most respects cluttered, it can be seen that the two saddle-node curves (which emanate from the different T.B. points) are connected by a codim 2 cusp bifurcation near the point labelled c (the cusp

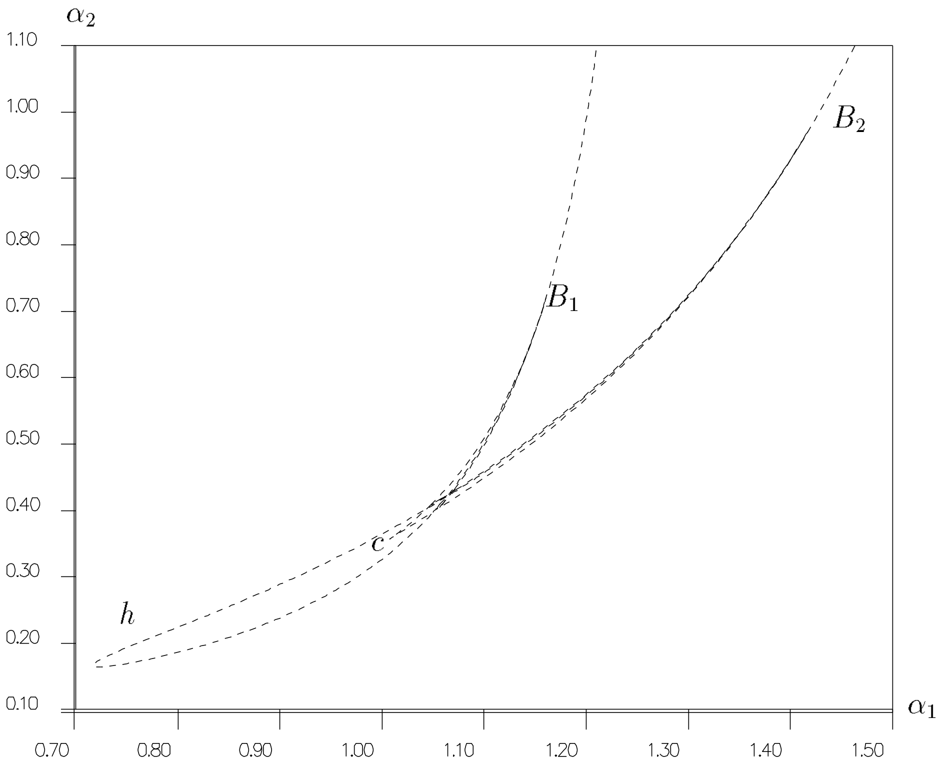

Figure 5: Projection onto the (α_1, α_2)-plane of the two-parameter bifurcation diagram for CO-oxidation.

appears as a turning point on the locus s in Figure 4).

The curves m_1 and m_2 are loci of homoclinic orbits to hyperbolic equilibria, starting points on which were found by following periodic orbits born at Hopf bifurcation points on h_1 and h_2 respectively. Note from Figure 6 that both loci of homoclinic orbits collide with saddle-node curves at points A_1 and A_2; $(\alpha_1, \alpha_2) = (1.04684, 0.40703)$ and $(1.05543, 0.40318)$. Homoclinic orbits at A_1 and A_2 are shown in Figure 7 (a)-(d) and Figure 8 (a)-(d). However, we found that we were *unable to successfully switch branches* to follow loci of codim 1 saddle-node homoclinic orbits at either A_1 or A_2. The reason for this is that the dynamics in the neighbourhood of A_1 and A_2 is not as simple as in Figure 1, because, surprisingly, we have found numerically that there are *at least two* distinct homoclinic orbits to the saddle-node at each of the points A_1 and A_2! The extra homoclinic orbit at A_1 is carefully plotted in Figure 7 (e)-(h) and that at A_2 is depicted in Figure 8 (e)-(h). In the captions of these figures, we have introduced a labelling of these homoclinic orbits according to the number position of local maxima in x and y of graphs of these orbits. We remark that the parameter values at which the two codim 2 homoclinic

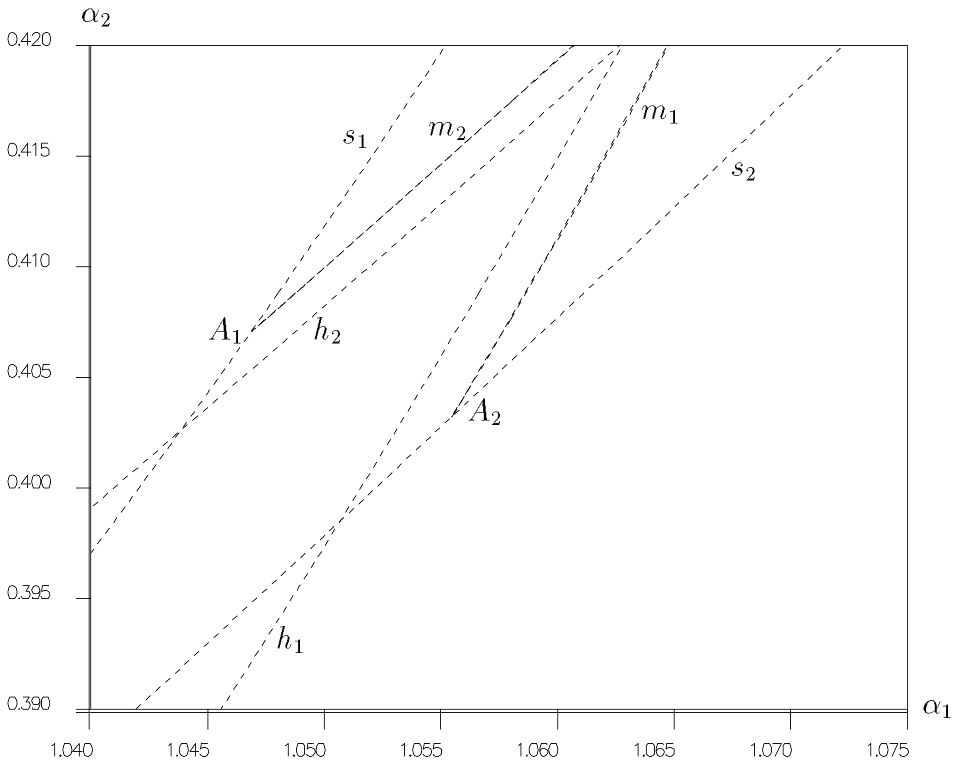

Figure 6: More detail of a small portion of the two-parameter bifurcation diagram for CO-oxidation.

orbits to saddle-nodes in Figure 7 (or 8) exist may not theoretically be exactly the same, but may differ by amounts smaller than the numerical error.

In fact, how we found the "other" homoclinic orbits at A_1 and A_2 was to compute loci of the non-trivial homoclinic orbits to hyperbolic equilibria, initial points on which were found by computing an isolated branch of periodic orbits that connects these two homoclinic orbits. Denote the values of α_i at points A_j by $\alpha_i^{(j)}$ $(i, j = 1, 2)$; namely $\alpha_i^{(j)} = \alpha_i(A_j)$. See Figure 6. We find numerically that for any fixed value of $\alpha_1 > \alpha_1^{(2)}$ (on the right-hand side of A_2), the periodic solution that bifurcates from the Hopf point on h_1 (resp. h_2) tends to the homoclinic orbits on m_1 (resp. m_2) as we follow the periodic solution to large period with parameter α_2 varying. Whereas, for $\alpha_1 < \alpha_1^{(1)}$ (on the left-hand side of A_1), periodic solutions bifurcating from the Hopf point on h_1 connect to the Hopf point on h_2. For the case of $\alpha_1^{(1)} < \alpha_1 < \alpha_1^{(2)}$ (i.e. between A_1 and A_2), upon following a periodic solution from a Hopf point on h_1 with fixed α_1 and increasing α_2 to a point where $\alpha_2 > alpha_2^{(1)}$, two new homoclinic orbits are obtained by fixing α_2 and doing continuation in α_1 in both directions. We have been able to follow loci of these two

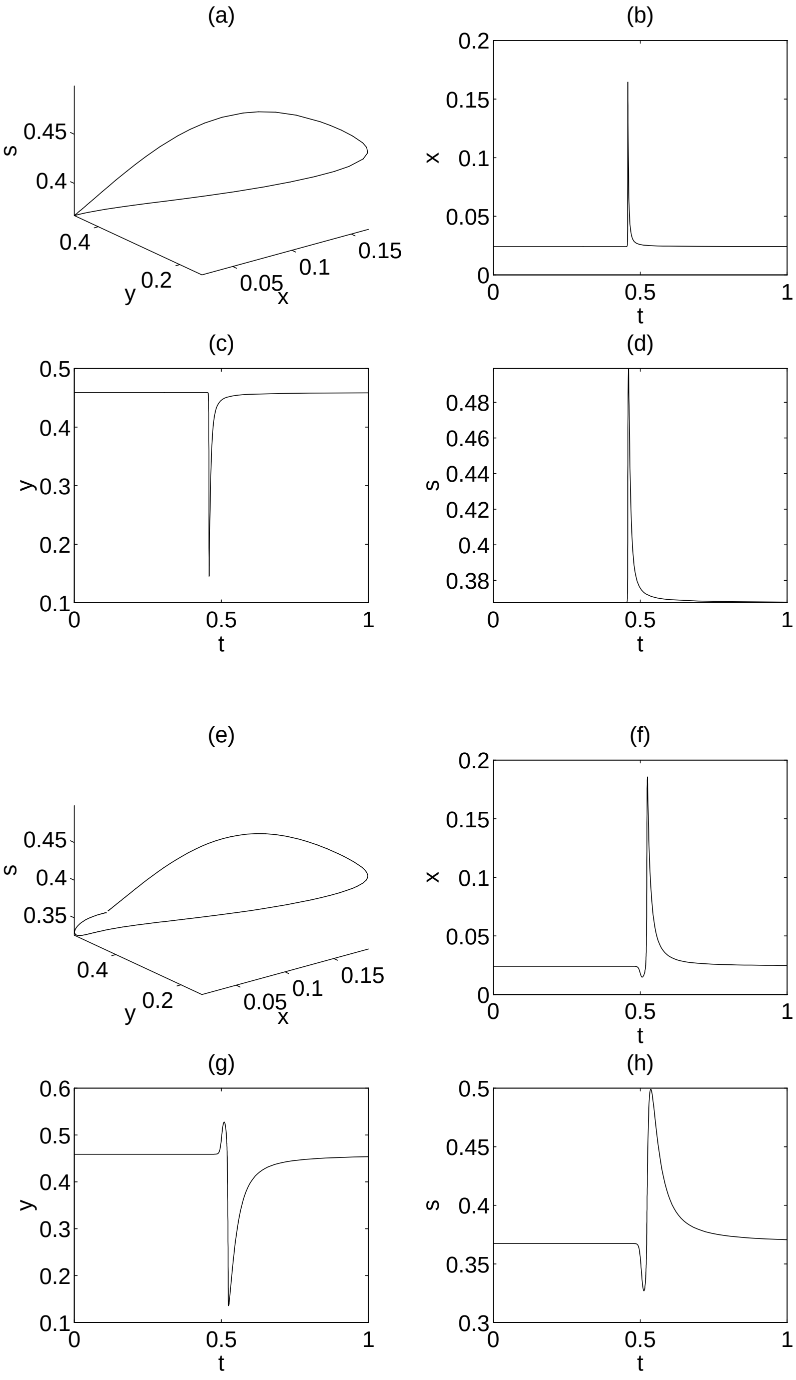

Figure 7: Homoclinic orbits for CO-oxidation at A_1. (a)–(d) The x-homoclinic orbit; here, and in subsequent figures, the time interval $T = 1.9 \times 10^4$ has been normalised to unity. (e)–(h) The yx-orbit, with $T = 3.5 \times 10^3$.

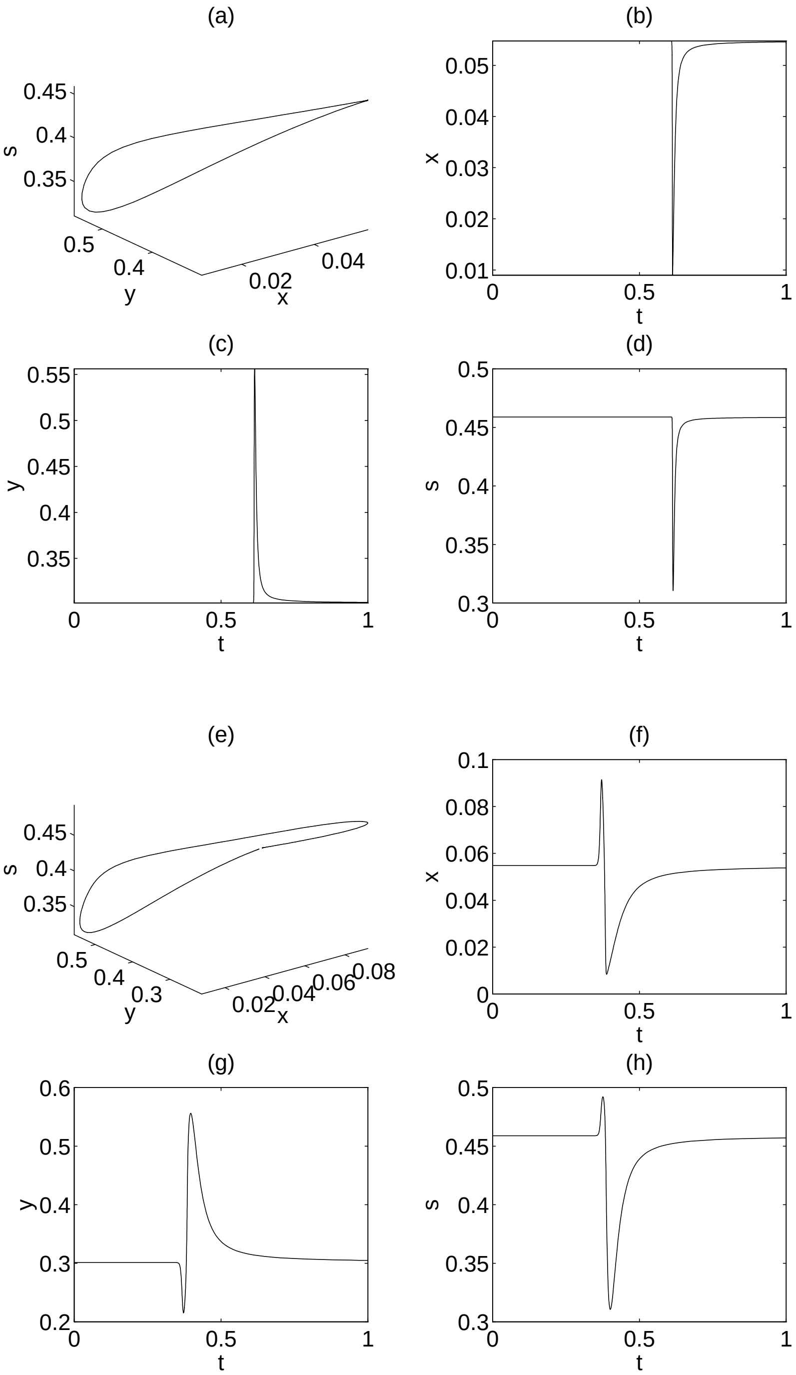

Figure 8: Homoclinic orbits for CO-oxidation at A_2; (a)–(d) the y-homoclinic orbit ($T = 2.4 \times 10^4$); (e)–(h) the yx-orbit ($T = 3.7 \times 10^3$).

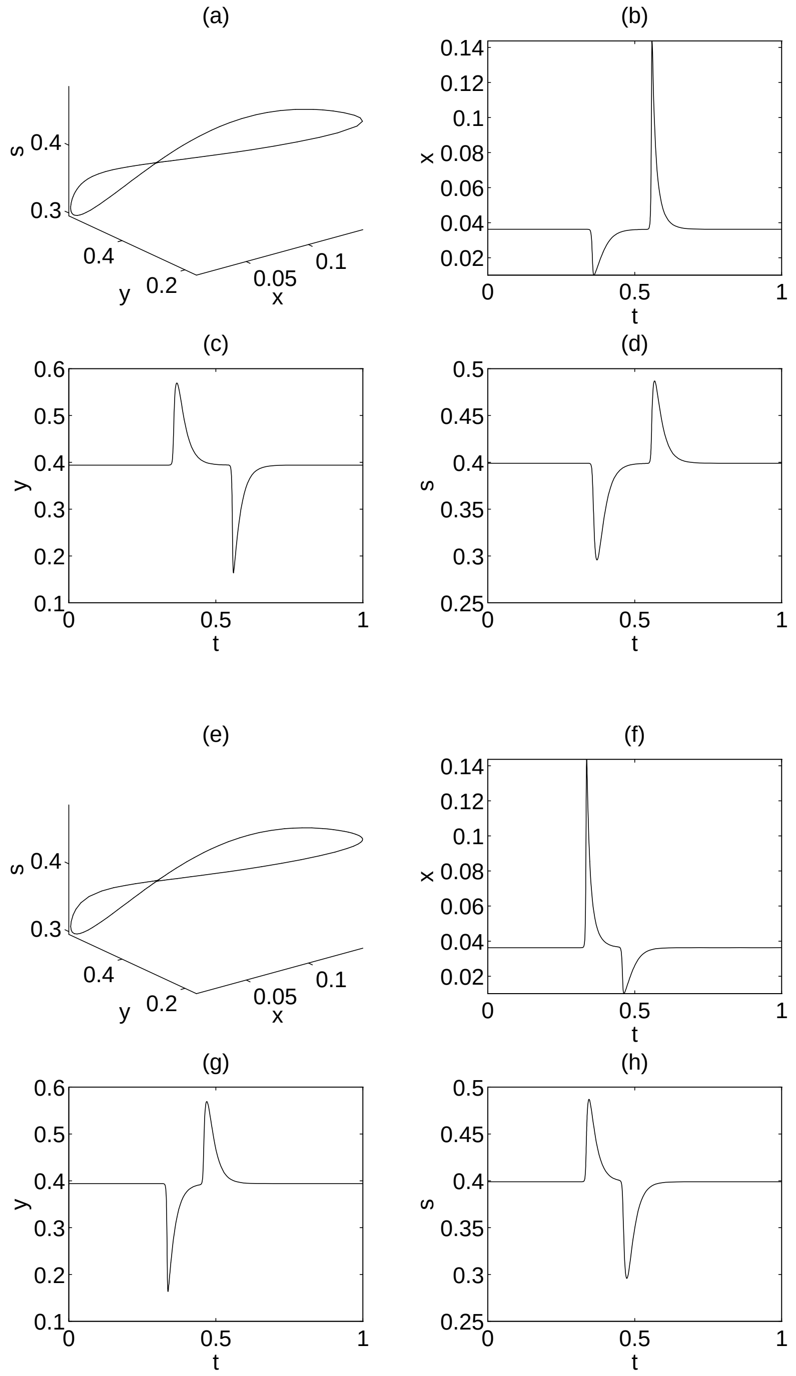

Figure 9: Homoclinic orbit for CO-oxidation at the codim 2 figure-of-eight bifurcation; (a)–(d) the xy-homoclinic orbit ($T = 3.5 \times 10^3$); (e)–(h) the yx-orbit ($T = 3.7 \times 10^3$).

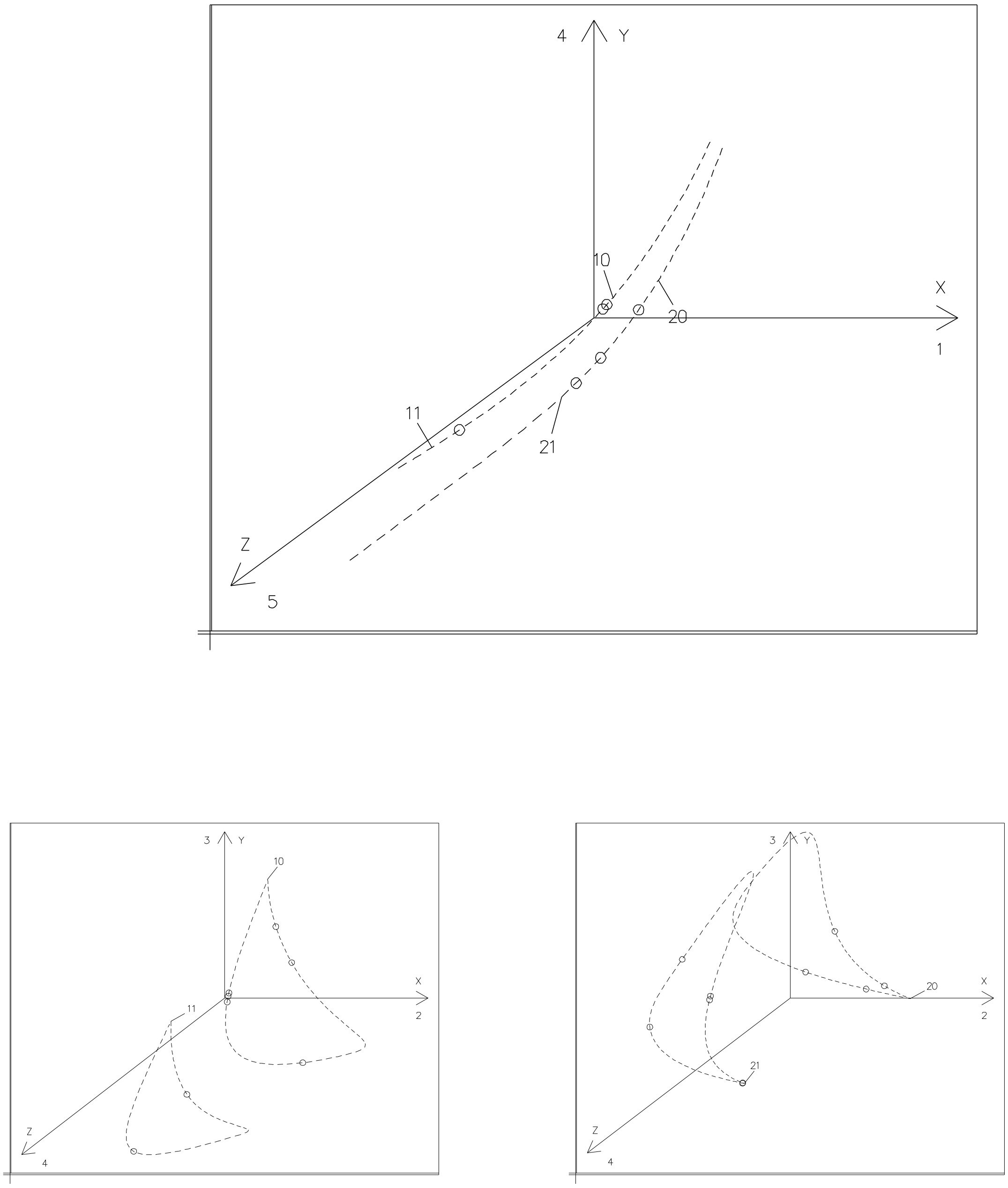

Figure 10: (a) Loci of codim 2 saddle-node homoclinic orbits in three parameters, in which $\alpha_1 \to x$, $\alpha_2 \to y$, $\alpha_3 \to z$; (b) (c) homoclinic orbits at the labelled points, in which $s \to z$.

non-trivial homoclinic orbits as they approach A_1 and A_2 and find that their loci are sufficiently close to m_2 and m_1 respectively to be numerically indistinguishable using the current methods. More interestingly, we have computed loci of the two non-trivial homoclinic orbits, starting from the same initial points, but in the opposite direction to that approaching A_1 and A_2. Both loci terminate at the point $(\alpha_1, \alpha_2) \approx (1.0687, 0.4276)$ at which the loci m_2 and m_1 cross (see Figure 4), remaining all the while numerically indistinguishable from m_1 and m_2. The point of collision between m_1 and m_2 is a another codim 2 homoclinic point, corresponding to a figure-of-eight "gluing bifurcation" between the x and y homoclinic orbits (see Glendinning (1988), Turaev & Shil'nikov (1987) and references therein). Our numerical algorithms cannot at present detect gluing bifurcations directly, because they involve the interaction of two independent homoclinic orbits. The two non-trivial homoclinic orbits near the figure-of-eight homoclinic point are shown in Figure 9. Note in comparison with Figures 7 and 8 that the time-interval between the "peak" and the "trough" of each of these orbits becomes large as the codim 2 point is approached and that the xy- and yx-orbits both tend to a copy of each of the x and y orbits.

We have also carried out continuation of the x and y codim 2 saddle-node homoclinic orbits in three free parameters, starting from A_1 and A_2 respectively. The third parameter is taken to be $\alpha_3 = k_3$, and, upon noting that both A_1 and A_2 are determined by a zero of the test function ϕ_9, we solve (3.1), (3.4)–(3.6) with the extra fixed condition

$$\phi_9 = 0,$$

(the second option mentioned at the end of Section 3.2). The results are given in shown in Figure 10, where (a) is bifurcation diagram in parameter space, (b) depicts homoclinic orbits from A_1 for $\alpha = (0.980152, 0.310457, 20.000000)$ and $(0.866228, 0.224992, 100.000000)$, and (c) depicts homoclinic orbits from A_2 for $\alpha = (1.012443, 0.321763, 20.000000)$ and $(0.956925, 0.256675, 100.000000)$.

5 Conclusion

In this paper we have demonstrated a new use of projection boundary conditions to compute codim 1 loci of saddle-node homoclinic orbits and in so doing treat codim 2 saddle-node homoclinic orbits in the same vein as other codim 2 points encountered on a locus of homoclinic orbits to hyperbolic equilibria. The drawback here is that, in order to continue through the degeneracy, one has to switch to a new system of boundary and defining conditions. The perhaps more interesting outcome of this paper is the ability to switch branches "the other way" from a curve of saddle node homoclinic orbits to a curve of hyperbolic homoclinic orbits, which global bifurcation cannot be detected by local properties of the equilibrium.

There remains much work to be done on the systematic numerical treatment of codim 2 homoclinic orbits. Quite apart from many known codim 2 singularities involving more than one homoclinic or heteroclinic connection (e.g. the gluing bifurcation encountered in Section 4.2), there remain many open questions (both theoretically and numerically) concerning potential codim 2 degeneracies occurring on loci of saddle-node homoclinic orbits. In this paper we have treated only one such codim 2 point, namely that corresponding to a termination of a locus of saddle-node homoclinic orbits, but, as is the case for hyperbolic homoclinic orbits, there are many possible (local or global) degeneracies which can potentially change the local qualitative dynamics but which do not cause the termination of the locus. Another possibility is that two or more homoclinic orbits exist that are asymptotic to the *same* saddle-node. This latter situation is of codimension-one for systems in three or more dimensions and was shown by Shil'nikov (1969) to imply Smale horseshoe dynamics.

There now follow some remarks on why we were unable to continue curves of codim 1 saddle-node homoclinic orbits for the example in Section 4.2. The situation is clearly complicated by the presence of more than one homoclinic orbit in a neighbourhood of the points A_i. From a theoretical point of view, it is unlikely that the yx- and xy- homoclinic orbits should describe exactly the same loci (m_1 and m_2 resp.) as the x- and y- homoclinic orbits. Indeed, the local theory at a figure-of-eight gluing bifurcation point (see Glendinning (1988), Turaev & Shil'nikov (1987) and references therein) suggests that the relevant loci should have a tangency of order δ, where δ is the ratio of the absolute values of the largest to the smallest leading real eigenvalues of the equilibrium. For the present example the eigenvalues at the figure-of-eight point are approximately $\mu_2 = -7.548$, $\mu_1 = -0.0113$ and $\lambda_1 = 0.1404$ (note that these parameter values do not satisfy the inequality assumed by Turaev & Shil'nikov (1987)). Hence $\delta \approx 12.4$ and, since the variation in parameter values between the points A_i and the figure-of-eight point are small, we expect that the theoretical loci of the yx- and and xy-homoclinic orbits should remain close to, but not identical with, the loci of the x- and y-homoclinic orbits respectively. It therefore seems likely that the the locus of homoclinic orbits in the neighbourhood of each point A_i forms a loop. For example, at A_1 the x-homoclinic orbit sticks onto the locus of saddle-nodes, a saddle-node homoclinic orbit exists for a tiny parameter range, and then it becomes unstuck to form the locus of yx-homoclinic orbits. We remark that this situation is consistent with our numerical inability to compute a locus of codim 1 saddle-node homoclinic orbits. Note finally that the dynamics represented in Figure 6 exist in a small portion of parameter space and are likely to be captured by normal-form analysis respective to a codim 3 bifurcation caused by the intersection of loci of cusp and Takens-Bogdanov bifurcations (cf. Bautin, (1975, 1977), Dumortier & Rousseau (1990) , Glendinning & Proctor (1994)), although we were unable to compute such a codim 3 point by following the points A_i in the three chosen parameters.

Acknowledgements

The research of both authors at Bath was supported by postdoctoral positions form the U.K. S.E.R.C. We are grateful to Yuri Kuznetsov for helpful comments.

References

Bautin, A. (1975), 'Qualitative investigation of a particular nonlinear system', *Appl. Math. Mech.* **39**, 606–615.

Bautin, A. (1977), 'On the nonlocal application of the method of small parameter', *Appl. Math. Mech.* **41**, 910–919.

Beyn, W.-J. (1990*a*), Global bifurcations and their numerical computation, *in* D. Roose, A. Spence & B. De Dier, eds, 'Continuation and Bifurcations: Numerical Techniques and Applications', Kluwer, Dordrecht, Netherlands, pp. 169–181.

Beyn, W.-J. (1990*b*), 'The numerical computation of connecting orbits in dynamical systems', IMA *J. Num. Anal.* **9**, 379–405.

Beyn, W.-J. (1992), Numerical analysis of homoclinic orbits emanating from a Takens-bogdanov point, Technical report, Sonderforschungbereich 343 Diskrete Strukturen in der Mathematik, Universitat Bielefeld. Preprint 92-065.

Bykov, V., Yablonski, G. & Kim, V. (1978), 'On one simple model of kinetic self-oscillations in catalytic reation of CO oxidation', *Dokl. Sov. Math* pp. 637–639.

Champneys, A. & Kuznetsov, Y. (1993), Numerical detection and continuation of codimension-two homoclinic bifurcations, Technical report, CWI, Amsterdam. To appear in *Int. J. Bifurcation & Chaos.*

Chow, S.-N. & Lin, X.-B. (1990), 'Bifurcation of a homoclinic orbit with a saddle-node equilibrium', *J. Diff. Int. Eqs.* **3**, 319–349.

Deng, B. (1990), 'Homoclinic bifurcations with nonhyperbolic equilibria', SIAM *J. Math. Anal.* **21**, 693–720.

Doedel, E. (1981), 'AUTO, a program for the automatic bifurcation analysis of autonomous systems', *Cong. Numer.* **30**, 265–384.

Doedel, E., Friedman, M. & Monteiro, A. (1993), On locating homoclinic and heteroclinic orbits, Technical report, Cornell Theroy Center; Center for Applied Mathematics, Cornell University.

Doedel, E., Keller, H. & Kernévez, J. (1991*a*), 'Numerical analysis and control of bifurcation problems: (I) Bifurcation in finite dimensions', *Int. J. Bifurcation and Chaos* **1**, 493–520.

Doedel, E., Keller, H. & Kernévez, J. (1991*b*), 'Numerical analysis and control of bifurcation problems: (II) Bifurcation in infinite dimensions', *Int. J. Bifurcation and Chaos* **1**, 745–772.

Dumortier, F. & Rousseau, C. (1990), 'Cubic Liénard equations with linear damping', *Nonlinearity* **3**, 1015–1039.

Friedman, M. (1993), 'Numerical analysis and accurate computation of heteroclinic orbits in the case of center manifolds.', *J. Dyn. Diff. Eqs* **5**, 59–87.

Friedman, M. & Doedel, E. (1991), 'Numerical computation and continuation of invariant manifolds connecting fixed points', SIAM *J. Numer. Anal.* **28**, 789–808.

Friedman, M. & Doedel, E. (1993), 'Computational methods for global analysis of homoclinic and heteroclinic orbits: A case study', *J. Dyn. Diff. Eqs.* **5**, 37–57.

Gaspard, P., Arnéodo, A., Kapral, R. & Sparrow, C., eds (1993), *Homoclinic Chaos*, *Physica D* **62**(1–4).

Glendinning, P. (1988), Global bifurcations in flows, *in* T. Bedford & J. Swift, eds, 'New Directions Dynamical Systems', C.U.P.

Glendinning, P. & Proctor, M. (1994), 'Travelling waves with spatially resonant forcing: bifurctions of a modified Landau equation', *Int. J. Bifurcation and Chaos* **3**, To appear.

Kaas-Peterson, C. & Scott, S. (1988), 'Homoclinic orbits in a simple chemical model of an autocatalytic reaction', *Physica D* **32**, 461–470.

Khibnik, A. (1990), LINBIF: A program for continuation and bifurcation analysis of equilibria up to codimension three, *in* D. Roose, A. Spence & B. De Dier, eds, 'Continuation and Bifurcations: Numerical Techniques and Applications', Kluwer, Dordrecht, Netherlands, pp. 283–296.

Lukyanov, V. (1982), 'Bifurcations of dynamical systems with a saddle-point separatrix loop', *Differential. Eq.* **18**, 1049–1059.

Schecter, S. (1987), 'The saddle-node separatrix-loop bifurcation', SIAM *J. Appl. Math.* **18**, 1142–1157.

Schecter, S. (1993), 'Numerical computation of saddle-node homoclinic bifurcation points', SIAM *J. Num. Anal.* **30**, 1155–1178.

Schecter, S. (1994), Rate of convergence of numerical approximations to homoclinic bifurcation points, North Carolina State University.

Shil'nikov, L. (1969), 'On a new type of bifurcation of multidimensional dynamical systems', *Sov. Math. Dokl.* **10**, 1368–1371.

Turaev, D. & Shil'nikov, L. (1987), 'On bifurcations of homoclinic 'figure eight' from a saddle with a negative saddle value', *Soviet. Math. Dokl.* **34**, 397–401.